J Porous Mater (2018) 25:137–146
DOI 10.1007/s10934-017-0427-9

A chromotropic acid modified SBA-15 as a highly sensitive fluorescent probe for determination of Fe^{3+} and I^- ions in water

Mehdi Karimi[1] · Alireza Badiei[1,2] · Negar Lashgari[1] · Ghodsi Mohammadi Ziarani[3]

Published online: 19 April 2017

Abstract A novel organic–inorganic hybrid nanomaterial (SBA-15-CA) was prepared by covalent immobilization of chromotropic acid onto the surface of mesoporous silica material SBA-15. Different techniques such as XRD, TEM, FT-IR, N_2 adsorption–desorption and TGA analyses were employed to characterize the grafting process. The data showed that the organic moiety (0.41 mmol g^{-1}) was successfully grafted to the SBA-15 and the primary hexagonally ordered mesoporous structure of SBA-15 was preserved after the grafting procedure. SBA-15-CA has been realized as a highly sensitive and selective fluorescent probe towards Fe^{3+} and I^- ions in aqueous media. SBA-15-CA exhibited a remarkable fluorescent quenching in the presence of Fe^{3+} ion over other competitive cations including Na^+, Mg^{2+}, Al^{3+}, K^+, Ca^{2+}, Cr^{3+}, Mn^{2+}, Fe^{2+}, Co^{2+}, Ni^{2+}, Cu^{2+}, Zn^{2+}, Cd^{2+}, Hg^{2+}, and Pb^{2+} as well as I^- ion among a series of anions including F^-, Cl^-, Br^-, CO_3^{2-}, HCO_3^-, CN^-, NO_3^-, NO_2^-, SCN^-, SO_4^{2-}, $H_2PO_4^-$, HPO_4^{2-}, and CH_3COO^-. A good linear response was observed between the concentration of the quenchers (Fe^{3+} and I^- ions) and fluorescence intensity of SBA-15-CA with detection limits of 1.5×10^{-7} M for Fe^{3+} and 0.2×10^{-7} M for I^-. Moreover, the effects of various pH values on the sensing ability of SBA-15-CA were investigated. Finally, the proposed method was successfully utilized for the determination of Fe^{3+} and I^- ions in river water, well water and tap water samples.

Keywords Organic–inorganic hybrid material · Functionalized SBA-15 · Fe^{3+} ion · I^- ion · Fluorescence

1 Introduction

During recent years, fluorescence sensing techniques have been intensively investigated by researchers in various fields in search for new fluorescent sensors capable of revealing presence of hazardous materials [1–5]. Fluorescent probes work based on transforming the changes in fluorescence emission when they bind to targets into the useful analytical signals. They offer ease in use and cost-effectiveness compared to the traditional techniques plus in most cases, they need simple preparation routes. So far, the most detected hazardous materials by means of fluorescent probes have been anions and metal cations [6, 7]. This remarkable focus on ions is due to the widespread use of anions and cations by industries such as metal plating, mining, fertilizers, tanneries, batteries, and pesticides. In addition, the lack of effective processes for elimination of ions from wastewaters, subsequently leads to releasing large amounts of them into the environment. On the other hand, since these ions are non-biodegradable, they can be accumulated in plants and animals and therefore, get into the human body through food chains. Among cations, it is recently known that beside essential roles played by Fe^{3+} ions in living organisms, unbalancing amount of this ion either being in higher level or lower level in the body has adverse effects such as anemia, diabetes, Alzheimer's disease and cardiac failure [8–10]. Among anions, iodide ion

✉ Alireza Badiei
abadiei@khayam.ut.ac.ir

[1] School of Chemistry, College of Science, University of Tehran, Tehran, Iran

[2] Nanobiomedicine Center of Excellence, Nanoscience and Nanotechnology Research Center, University of Tehran, Tehran, Iran

[3] Department of Chemistry, Faculty of Science, Alzahra University, Tehran, Iran

plays an important role in human growth and health via thyroid function and neurological activity. It has also been known that both deficiency and excess intake of iodide can lead to a variety of diseases such as metabolic disorders and even brain damage [11–13]. Up to now, some successful reports have been published declaring detection of Fe^{3+} [14–17] and I^- [18–20] individually. However, there are lots of reported probes for these ions which suffer from some disadvantages like requiring tedious synthetic procedures [21, 22] or organic solvents for optimal sensing performance which makes them inapplicable for direct utilizing in water samples [23–29]. Therefore, it is of importance to design and fabricate a novel fluorescent probe capable of detecting these two opposite ions, i.e. Fe^{3+} and I^-, in 100% aqueous solution which is also technologically and economically more interesting. To the best of our knowledge, there is only one report on a small organic probe capable of detecting these two ions, however, it requires organic solvents (THF and CH_3CN) [30].

As a new class of fluorescent probes, organic–inorganic hybrid nanomaterials have attracted particular attention. Generally, the organic part in this class consists of a binding site which selectively coordinate to a specific analyte and a fluorophore which is responsible for emitting light. The inorganic part provides high surface area acting as an excellent support for the attachment of organic part. Different inorganic host materials that have been frequently utilized for developing functional materials include core–shell nanomaterials [31], SiO_2 nanoparticles [32], mesocage scaffolds [33] and ordered nanoporous silica (ONS) materials such as MCM-41 [34], SBA-15 [35], and LUS-1 [36]. Among the mentioned scaffolds, ONS materials have been the most chosen ones by researchers because they offer versatile characteristics. ONS materials possess a high specific surface area covered with abundant hydroxyl groups (−OH) accessible for grafting of organic moieties. The presence of large ordered channels with two open ends and large pore diameters facilitate the movements of ions through the channels. Due to the presence of hydroxyl groups all over the surface, the surface becomes polar and water molecules can move easily in and out to the pores. Therefore, ONS materials make it possible for attachments of even the water insoluble organic moieties onto the surface and applied them in aqueous media without using organic solvents. These materials are transparent in a wide range of UV–Vis region, so no interferences are made by them on the fluorescence spectra. Since the organic moieties are covalently bounded to the surface, bleaching out of these groups into the solution is hindered and photostability of fluorophores are also improved. Thus they become more durable for a long time and for a successive recycling and usages. Finally, bio-compatibility of ONS materials makes them suitable for being used in aquatic environments.

A number of methods such as atomic absorption spectrometry [37, 38], inductively coupled plasma-mass spectroscopy (ICP-MS) [39, 40], and voltammetry [41, 42] have been used for detection and estimation of Fe^{3+} and I^- ions in solutions. However, these methods are extremely costly, time consuming, nonportable and employ complicated instrumental calibrations, sample pretreatments and well-trained operators. In contrast, optical probes benefit from low costs, simplicity, real-time monitoring with fast response time, high selectivity and sensitivity.

Recently, our research group has focused in search for new chemosensors based on ONS materials and a number of fluorescent chemosensors have been designed and reported [43–48]. Herein, in continuation of our attempts, we intend to introduce a novel SBA-15 based fluorescent chemosensor (SBA-15-CA) capable of detecting two opposite ions. SBA-15-CA exhibited a remarkable fluorescent quenching in the presence of Fe^{3+} ion over other competitive cations including Na^+, Mg^{2+}, Al^{3+}, K^+, Ca^{2+}, Cr^{3+}, Mn^{2+}, Fe^{2+}, Co^{2+}, Ni^{2+}, Cu^{2+}, Zn^{2+}, Cd^{2+}, Hg^{2+}, and Pb^{2+} as well as I^- ion among a series of anions including F^-, Cl^-, Br^-, CO_3^{2-}, HCO_3^-, CN^-, NO_3^-, NO_2^-, SCN^-, SO_4^{2-}, $H_2PO_4^-$, HPO_4^{2-}, and CH_3COO^-. SBA-15-CA was prepared through two-step post-grafting method, i.e. functionalization of SBA-15 surface with 3-(idoopropyl)triethoxysilane followed by covalent attachment of chromotropic acid groups. We show that this probe demonstrates beneficial properties, such as high sensitivity and selectivity towards Fe^{3+} and I^- ions in total aqueous media, its detection limit values are comparable to purely organic-based probes reported in the literature, it is applicable in real water samples and its preparation method is simple.

2 Experimental

2.1 Materials and instruments

Tetraethylorthosilicate (TEOS, Merck) and Pluronic P123 ($EO_{20}PO_{70}EO_{20}$, MW = *ca.* 5800) (Aldrich) were used as a silica source and structure-directing agent, respectively. 3-(Idoopropyl)triethoxysilane (CITES, Merck), 1,8-dihydroxynaphthalene-3,6-disulfonic acid disodium salt (chromotropic acid, Merck), hydrochloric acid (Merck), THF (Merck), triethylamine (TEA, Merck) and all other materials including metal salts were purchased from Merck and Sigma–Aldrich and used without further purification.

Low-angle X-ray diffraction (LAXRD) measurements were performed on X'Pert Pro MPD diffractometer using Cu K_α radiation ($\lambda = 1.5418$ Å). The N_2 adsorption–desorption isotherms were obtained using a BELSORP-miniII instrument at liquid nitrogen temperature (−196 °C). All samples were degassed at 100 °C before performing

measurements. The Brunauer-Emmett-Teller and Barrett-Joyner-Halenda equations were applied on sorption data using BELSORP analysis software to calculate physical properties of materials such as specific surface area, pore diameter, pore volume and pore size distribution. The Fourier transform infrared (FT-IR) spectra were obtained in KBr disks on a RAYLEIGH WQF-510A. Transmission electron microscopy (TEM) was performed using a Zeiss EM900 instrument at an accelerating voltage of 80 kV. Samples were dispersed in ethanol using an ultrasonic bath and a drop of the ethanol mixture was placed on a lacey carbon-coated copper grid for analysis. FESEM images were obtained on MIRA3 microscope. Thermogravimetric analyzes (TGA) were carried out by a TGA Q50 V6.3 Build 189 instrument from ambient temperature to 800 °C with a ramp rate of 10 °C min^{-1} in the air. Fluorescence measurements were collected on a Cary Eclipse Fluorescent Spectrophotometer.

2.2 Synthesis of iodo functionalized SBA-15 (SBA-15-I)

SBA-15 was synthesized according to ref [49]. Typically, pre-dried SBA-15 (2 g) was dispersed in THF in a two-neck container for about 0.5 h to gain a homogeneous dispersion. Then, CITES (10 mmol) was added to the solution and the mixture was refluxed overnight. The resultant solid (denoted as SBA-15-I) was filtered, washed with toluene and THF, and dried over night at ambient temperature.

2.3 Synthesis of chromotropic acid functionalized SBA-15 (SBA-15-CA)

After the homogeneous dispersion of SBA-15-I (1 g) in THF, the mixture of chromotropic acid (5 mmol) and TEA (5 mmol) in THF was added to the solution together with vigorous stirring and the mixture was refluxed for 6 h. After that, the solid product was filtered, washed with THF and methanol, and finally dried overnight in oven at 80 °C. The final product was denoted as SBA-15-CA. Scheme 1 depicts the synthetic procedure of SBA-15-I and SBA-15-CA.

2.4 The fluorescence experimental procedures

All the experiments were conducted in double distilled pure water. Stock solutions of all metal-ions (1×10^{-2} M) were prepared using their nitrate salts. Those of anions (1×10^{-2} M) were prepared using their sodium or potassium salts. For the preparation of a stock solution of SBA-15-CA, 0.02 g of the fine powder of SBA-15-CA was added to 100 mL of double distilled pure water and the solution was dispersed under sonication to ensure the rapid mixing. The volume of a solution of SBA-15-CA used in all experiments was 3 mL brought into a fluorescence quartz cell 10 mm for measurement. All tests were carried out at room temperature. 1 min was selected as the detection time in this paper.

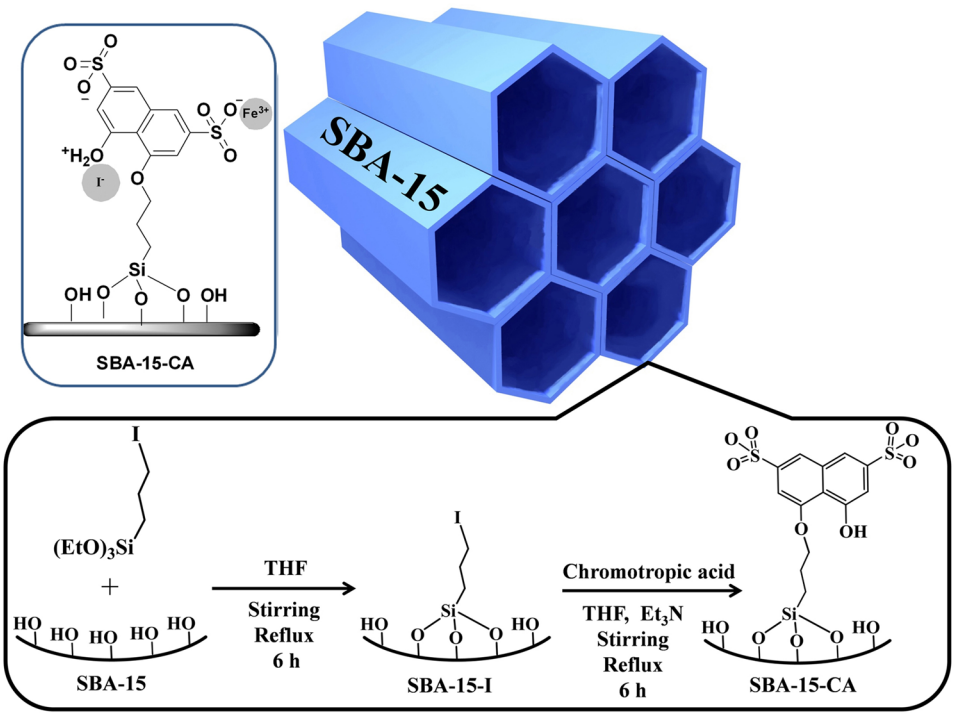

Scheme 1 The synthetic procedure of SBA-15-CA and proposed binding mechanism of SBA-15-CA for Fe^{3+} and I^- ions

The ion recognition behavior of SBA-15-CA was evaluated from the changes in fluorescence spectra of SBA-15-CA (3 mL H_2O suspension, 0.2 g L^{-1}) upon addition of 33 µM that ion. Titration spectra were recorded by adding different concentrations of Fe^{3+} and I^-ions to 3 mL of SBA-15-CA solution to quench the fluorescence.

To evaluate any possible interference due to different metal ions for the estimation of Fe^{3+} and different anions for the estimation of I^- ion, the measurements were made according to the following procedure. In a fluorescence quartz cell 10 mm, 3 mL of the stock solution of SBA-15-CA (0.2 g L^{-1}) and Fe^{3+} ion along with other interfering metal ions (in a 1:4 ratio) were mixed and then, the fluorescence intensity of each solution was recorded. The same procedure was reported for I^- ion in the presence of interfering anions.

To study the possible effects of pH, hydrochloric acid and sodium hydroxide were employed to adjust pH values. After each adjustment of pH, the fluorescence spectra of the stock solution of SBA-15-CA (3 mL, 0.2 g L^{-1}) were individually recorded in absence and presence of Fe^{3+} and I^- ions (33 µM).

3 Results and discussions

3.1 Characterizations

Figure 1 shows FESEM (a) and TEM (b) images of original SBA-15 particles. FESEM displayed rod-type external morphology of particles and TEM images showed long parallel channel-structure throughout the particles.

Figure 2 illustrates the LAXRD patterns of original SBA-15 and final product of SBA-15-CA. Generally, ONS materials exhibit three characteristic reflections in LAXRD patterns: one intense reflection at the 2θ value around 0.9

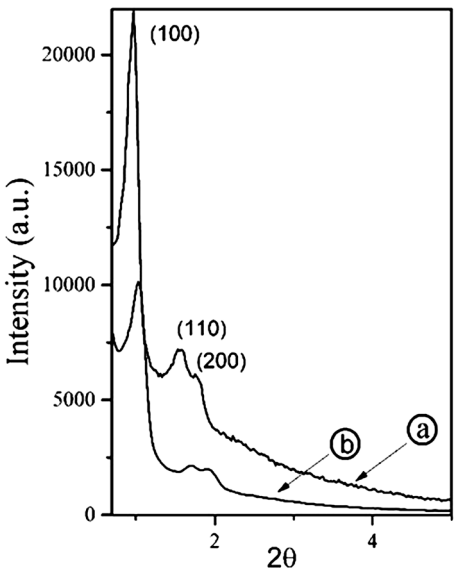

Fig. 2 LAXRD patterns of *a* SBA-15 and *b* SBA-15-CA

related to the diffraction from (100) plane and 2 weak reflections at 2θ value near 1.9 attributed to the diffraction from (110) and (200) planes. The observation of those above mentioned reflections in LAXRD patterns of samples imply the presence of long range order and 2D-hexagonal mesostructure. As can be seen in Fig. 2a, b, LAXRD patterns of both samples exhibited these characteristics reflections which mean the maintenance of the structural properties of original SBA-15 after modification steps. However, the intensity of those reflections was decreased for functionalized sample, i.e. SBA-15-CA, indicating the presence of organic components covalently grafted into the pore channels may decrease the mesoscopic order of the pore channels, leading to the decreased intensity of (1 0 0), (1 1 0), and (2 0 0) reflections.

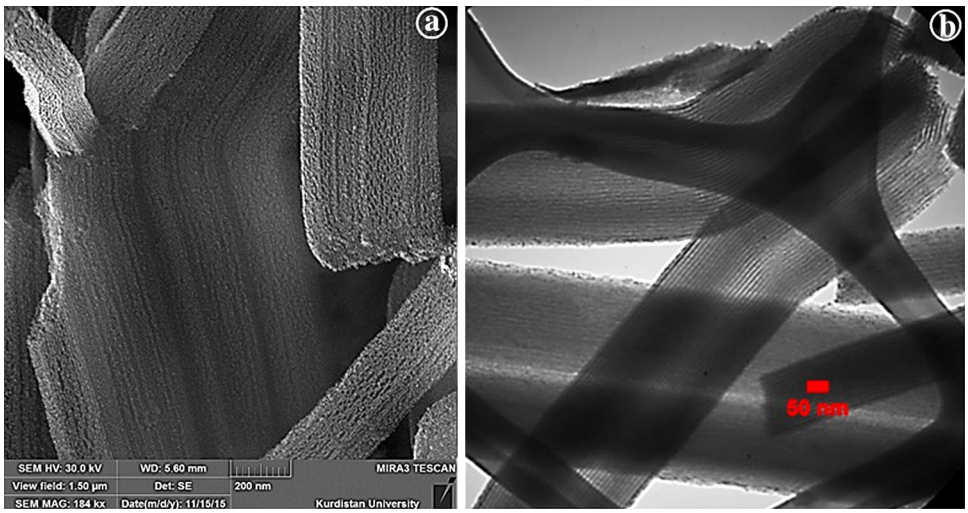

Fig. 1 **a** FESEM and **b** TEM images of original SBA-15

Figure 3 demonstrates N_2 adsorption–desorption isotherms of SBA-15 and SBA-15-CA. Both samples exhibited a type IV standard IUPAC isotherm which corresponds to mesoporous materials. The hysteresis loop between P/P_0 at 0.5–0.8 was characteristics of large tubular pores [50]. As it can be seen from the structural properties of samples in the inset of Fig. 3, the amount of all three parameters, i.e. specific surface area, average pore diameter, and total pore volume, were decreased for SBA-15-CA which were due to grafting organic moieties onto the surface of SBA-15 resulting in lowering the volume of adsorbed N_2 molecules into the pores. Furthermore, the similarity between the isotherms for both samples confirmed that the original structure of SBA-15 was not collapsed which is in accordance with LAXRD results.

In order to further supporting the attachment of fluorophores, FT-IR spectra of SBA-15 and SBA-15-CA were recorded. As shown in Fig. 4, SBA-15 spectrum showed characteristic peaks of mesoporous silica materials which were also observed for SBA-15-CA including peaks around 800 and 1100 cm^{-1} (Si–O–Si framework stretching vibrations), a wide band above 3000 cm^{-1} (O–H vibrational stretching) which was decreased for SBA-15-CA due to the functionalization, and a peak around 960 cm^{-1} (Si–O–H bending stretching). In addition, SBA-15-CA spectrum showed peaks within the range of 2880–2995 cm^{-1} attributed to aliphatic C–H stretching vibrations, and a series of peaks around 1208, 1370 and 1605 cm^{-1} could be assigned to the sterching vibration of C-Si, asymmetric stretching of S=O bands of sulfonate groups and C=C streching in aromatic ring, respectively. Moreover, a peak around 1640 cm^{-1} could be due to the physisorbed water molecules.

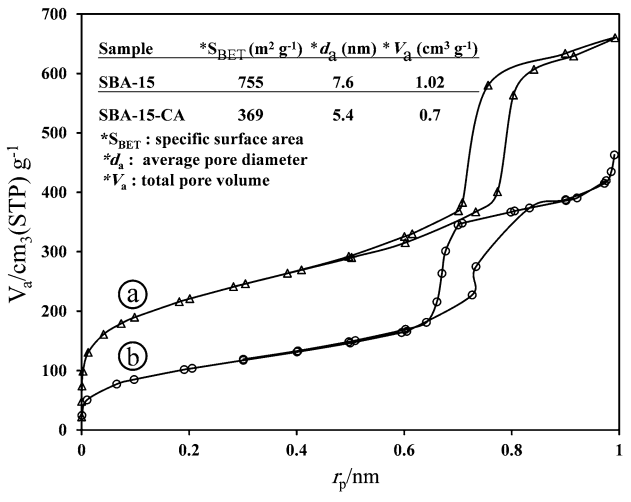

Fig. 3 N_2 adsorption–desorption isotherms of *a* SBA-15 and *b* SBA-15-CA. *Inset* is the table of structrul parameters

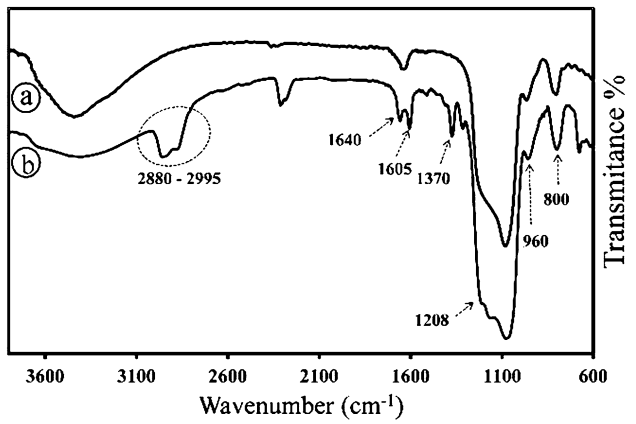

Fig. 4 FT-IR spectra of *a* SBA-15 and *b* SBA-15-CA

Figure 5 gives thermogravimetric curves of SBA-15-I and SBA-15-CA which were taken to measure the quantity of the attached organic moieties. The weight loss up to 150 °C can be assigned to the elimination of physiosorbed water molecules. Moreover, the weight loss between 150 and 650 °C can be attributed to the degradation of organic moieties. Therefore, the amount of the attached organic mieoties on the surface of SBA-15 was about 7 and 12% for SBA-15-I and SBA-15-CA, respectively. Based on these percentages, the amount of the attached fluorophore was approximately estimated to be 0.41 mmol g^{-1}.

3.2 Fluorescence response of SBA-15-CA

The fluorescence properties of SBA-15-CA were separately evaluated in presence of various cations and anions. A number of common cations including Na^+, Mg^{2+}, Al^{3+}, K^+, Ca^{2+}, Cr^{3+}, Mn^{2+}, Fe^{2+}, Fe^{3+}, Co^{2+}, Ni^{2+}, Cu^{2+}, Zn^{2+}, Cd^{2+}, Hg^{2+}, and Pb^{2+} and a series of anions including F^-,

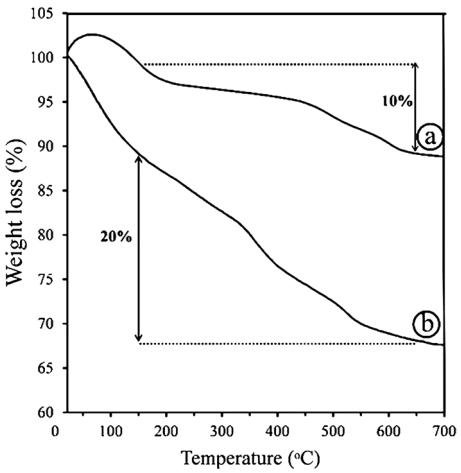

Fig. 5 TGA curves of *a* SBA-15-I and *b* SBA-15-CA

Cl^-, Br^-, I^-, CO_3^{2-}, HCO_3^-, CN^-, NO_3^-, NO_2^-, SCN^-, SO_4^{2-}, $H_2PO_4^-$, HPO_4^{2-}, and CH_3COO^- were investigated. These two types of ions were evaluated in different excitation wavelengths in order to find the best results in terms of sensing behavior. It was found that applying the wavelength of 315 nm as excitation wavelength for cations and 235 nm for anions resulted in the optimum responses. The aqueous suspended SBA-15-CA followed by excitation at both excitation wavelengths showed an intense emission within the range of 300–450 nm. Figure 6 depicts the recorded changes in emission of the probe. As can be seen in Fig. 6a, all the cations except for Fe^{3+} had little impact on the fluorescence emission of SBA-15-CA whereas upon the addition of Fe^{3+} ion, the emission was remarkably quenched. The interesting point is that despite the very similar system which was reported in ref. [51], Hg^{2+} ion did not affect the emission of the present sensing system. On the other hand, for anions experiments, the significant quench of fluorescence emission was only observed upon addition of I^- ion and the impact of other anoins was negligible, as it is depicted in Fig. 6b.

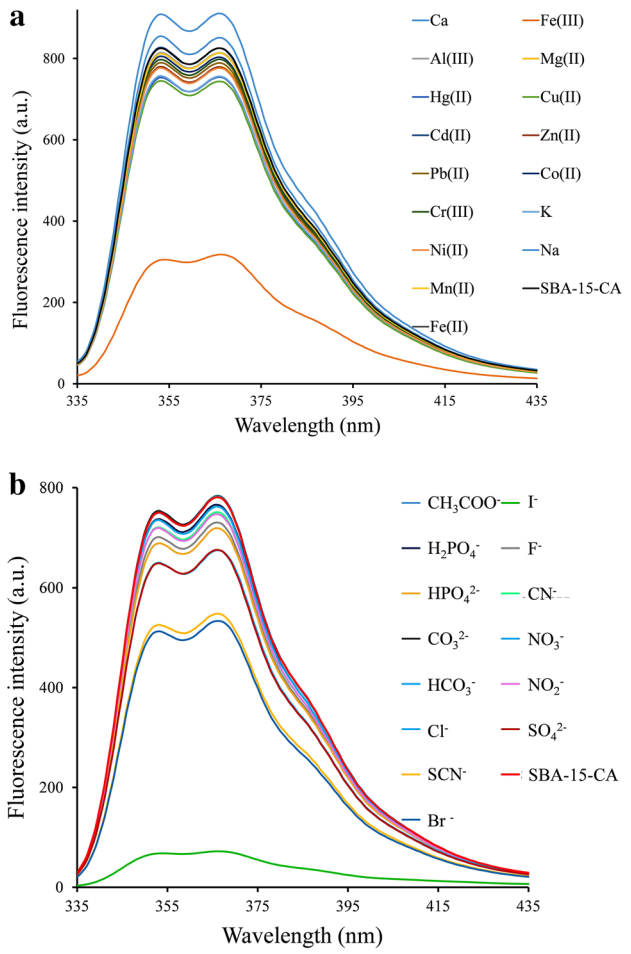

Fig. 6 Fluorescence emission spectra of SBA-15-CA (3 mL H_2O suspension, 0.2 g L^{-1}, pH = 6) in the presence of 33 μM **a** Na^+, Al^{3+}, Mg^{2+}, Ca^{2+}, K^+, Cr^{3+}, Mn^{2+}, Fe^{2+}, Fe^{3+}, Co^{2+}, Ni^{2+}, Cu^{2+}, Zn^{2+}, Cd^{2+}, Hg^{2+}, and Pb^{2+} ions (λ_{ex} = 315 nm) and **b** F^-, Cl^-, Br^-, I^-, CN^-, NO_2^-, NO_3^-, SO_4^{2-}, CO_3^{2-}, HCO_3^-, $H_2PO_4^-$, HPO_4^{2-}, SCN^-, CH_3COO^- ions (λ_{ex} = 235 nm)

3.3 pH Effects

In order to provide the optimum condition for fluorescence measurements, the evaluation of SBA-15-CA efficiency in a wide pH range was studied. The effects of various pH ranging from 2 to 12 on the fluorescence intensity of SBA-15-CA was recorded in the absence and presence of Fe^{3+} and I^- ions, individually. The fluorescence intensity of SBA-15-CA in absence and presence of I^- ions were almost independent from pH values indicating that SBA-15-CA is an excellent probe for detection of iodide over a wide pH range from 2 to 12. However, the fluorescence intensity of SBA-15-CA in the presence of Fe^{3+} was unstable and it can be used as a Fe^{3+}-probe in pH values in the range of 4–8 (Fig. 7). This pH insensitivity of SBA-15-CA in near neutral media is of importance for its practical applications in both environmental and biological analysis. For further studies, the pH of solvent kept constant at 6.

3.4 Fluorescence competition study

The selectivity of the probe toward Fe^{3+} and I^- ions in the presence of other ions as interfering agents is an extremely important feature that should be investigated. Accordingly, the competition experiments were conducted and the results were depicted in Fig. 8. As it can be seen, negligible interfering effects were observed for both ions implying that SBA-15-CA is a selective sensing system for detection of these two ions even in the presence of excess amounts of other ions.

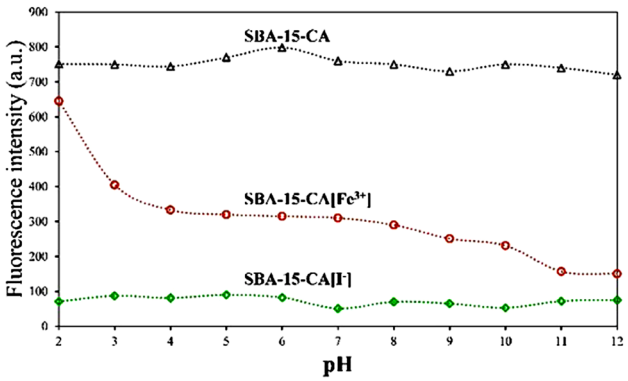

Fig. 7 Effect of pH on the fluorescence response of SBA-15-CA (3 mL H_2O suspension, 0.2 g L^{-1}) in absence and presence of the quenchers (33 μM)

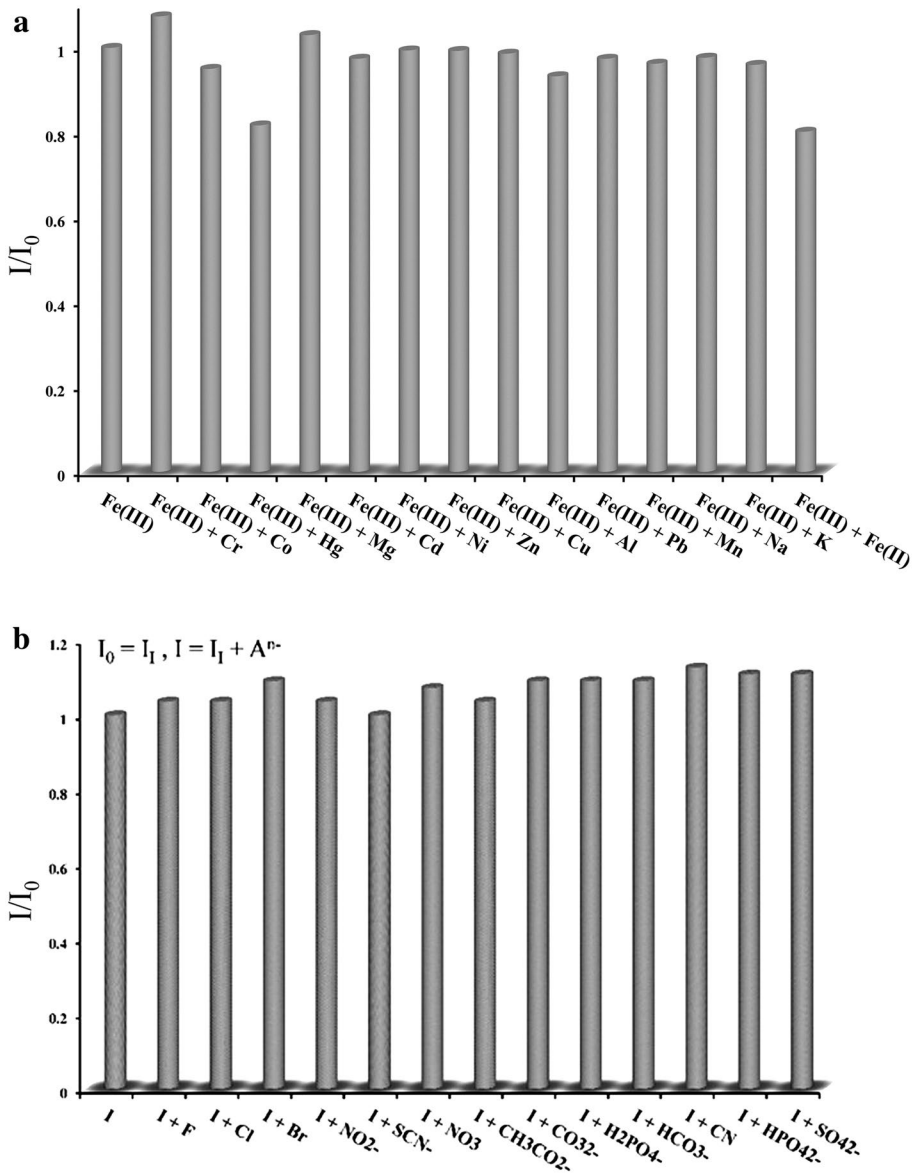

Fig. 8 Selectivity of SBA-15-CA (3 mL H_2O suspension, 0.2 g L^{-1}, pH = 6) for **a** Fe^{3+} ion (λ_{ex} = 315 nm) and **b** I^- ion (λ_{ex} = 235 nm) in the presence of other related ions as interfering agents. ([Fe^{3+}] or [I^-] to [other ions] = 1:4)

3.5 Fluorescence titration study and detection limits

To determine the sensitivity of the probe towards different concentrations of Fe^{3+} and I^- ions and also to infer the mechanism of fluorescence quenching, fluorescence titration experiments were performed. As shown in Fig. 9, similar quenching behavior was observed as gradual increase in concentration of both ions, but the quenching effect of iodide was slightly more than Fe^{3+} ions. Moreover, plotting the fluorescence intensities against the concentration of the quenchers ([Q]) revealed that these two parameters were linearly related to each other for concentrations below 25 μM (Fig. 10). This means that the static quenching mechanism happened and the fluorophores were equally accessible to quenchers [29, 52] supported by the fact that fluorophores were immobilized on the surface of SBA-15 and molecular translational motion for them was hindered. Therefore, Stern–Volmer equation can be applied which is stated as $I_0/I = 1 + K_{sv}[Q]$, where I_0 and I represent the intensity of the probe in absence and presence of the quencher, respectively, and K_{sv} is the Stern–Volmer constant providing quantitative measure of quenching. K_{sv} was found to be 1.6×10^7 and 2.0×10^7 M^{-1} for Fe^{3+} and I^-, respectively. Furthermore, the deviation from linearity for [Q] was observed for concentrations higher than 25 μM and it could be possibly due to binding of ions to the grafted fluorophores mostly on the entrance of the pores which made the penetration of the rest of the quencher into the inner part difficult and thus, interior flourophores became inaccessible to the quenchers. The detection limit (D_L)

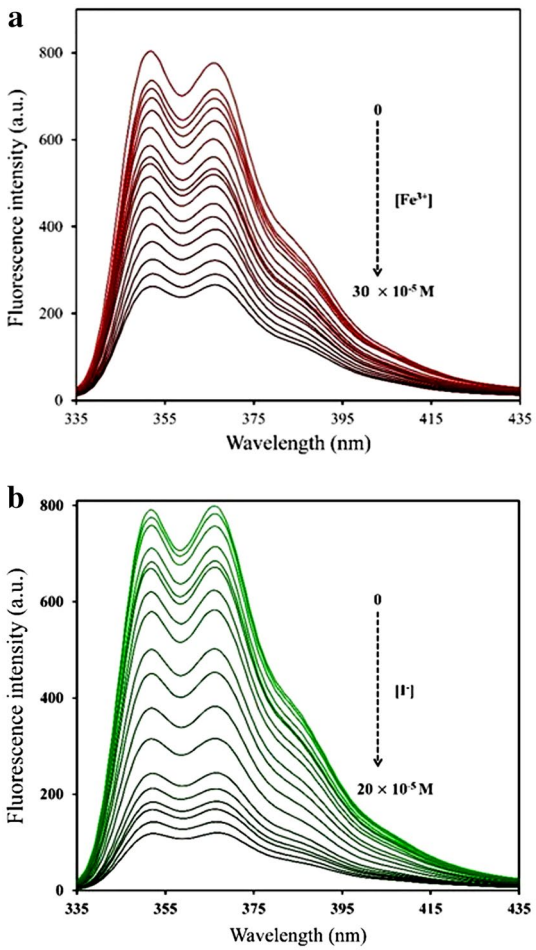

Fig. 9 Fluorescence emission spectra of SBA-15-CA (3 mL H_2O suspension, 0.2 g L^{-1}, pH = 6) upon addition of increasing concentrations of **a** Fe^{3+} ion (λ_{ex} = 315 nm) and **b** I^- ion (λ_{ex} = 235 nm)

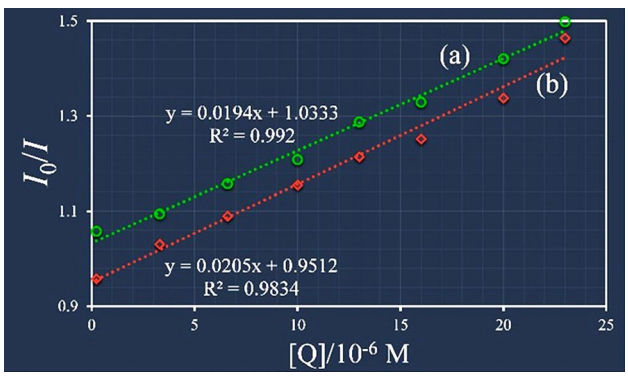

Fig. 10 Fluorescence intensity ratio of I_0/I as a function of quencher concentration ([Q]). *a* Fe^{3+} and *b* I^- ion (I_0 and I = Fluorescence intensity of SBA-15-CA in absence and presence of quencher, respectively)

of the proposed probe for both ions was calculated using the following equation: $D_L = 3\sigma/m$ where σ represents the standard deviation of the blank solution measured six times and m is the slope of the fluorescence intensity *versus* [Q]. D_L was calculated to be 1.5×10^{-7} M for Fe^{3+} and 0.2×10^{-7} M for I^- ion.

Additionally, the performances of a series of chemosensors for the detection of Fe^{3+} are listed in Table 1. As is evident from Table 1, compared with other chemosensors, SBA-15-CA is one of a few probes that work in total aqueous media. Also, the detection limit result obtained for SBA-15-CA is comparable to the reported values in the literature, as shown in Table 1.

3.6 Mechanisms of fluorescence quenching

As discussed before, both Fe^{3+} and I^- ions resulted in quenching of fluorescence emission of naphthalene units. Considering the observed linearity of the fluorescence intensity toward the concentrations of both ions, static quenching mechanism was proposed implying the formation of a non-fluorescent complex between the ions and fluorophores. In the case of Fe^{3+} ion, it is proposed that the quenching effect could be due to the paramagnetic nature of Fe^{3+} ions with unpaired electron in d^5 electronic configuration which could give rise to an intramolecular electron transfer or energy transfer processes between ligand and Fe^{3+} within the complex. Because of the charge, Fe^{3+} ions are more probably bind to sulfonic groups (Scheme 1) [14, 61, 62]. On the other hand, iodide is well-known to impose heavy atom effect on fluorescence emission. When iodide binds to the fluorephores, it quenches the emission via intersystem crossing induced by spin–orbit coupling upon interaction with the excited state of the fluorophore. In other words, the excited fluorpophores are returned to the ground state by non-radiative decay. As the case of Fe^{3+}, static quenching mechanism was also observed for iodide ion [1, 29, 52]. Interestingly, iodide was also an effective quencher in previously reported fluorescent system in ref [47]. in which fluorophore was also contained sulfonic groups. Therefore, it was proposed that some degree of the anion-π interaction could be involve between I^- ion and naphthalene ring [63, 64].

3.7 Real samples

SBA-15-CA was successfully applied in three different types of water (tap water, well water and river water of Tehran) for the detection of Fe^{3+} and I^- ions. River water and well water were filtered through a filter paper before use. After dispersing SBA-15-CA in each sample, the fluorescence intensity spectra of the prepared samples were recorded. Then, the samples were spiked with known amounts of Fe^{3+} and I^- ions and their emissions were analyzed. Table 2 summarizes the results derived from the recorded fluorescence spectra after the addition of Fe^{3+} and

Table 1 A comparison of the performance of SBA-15-CA with some reported chemosensors

No.	Structure	Detection limit	Medium	Ref.
1	Benzimidazole-based tripodal receptor	2.1×10^{-5}	CH_3CN	[53]
2	2-(4-(2,2′-Bipyridin-5-yl)phenyl)-1*H*-phenanthro[9,10-*d*]imidazole	5.26×10^{-6}	MeOH/H_2O (1/1)	[54]
3	Chalcone-based chemosensor	3.49×10^{-6}	DMSO/H_2O (1/1)	[55]
4	Rhodamine-based probe	5×10^{-6}	MeOH/H_2O (4.5/5.5)	[56]
5	Tyloxapol	2.2×10^{-6}	H_2O	[57]
6	8-Hydroxyquinoline-based chemosensor	5.6×10^{-7}	EtOH/THF (99:1)	[58]
7	LQS[a]	4.2×10^{-6}	H_2O	[36]
8	SBA-F[b]	1.35×10^{-5}	H_2O	[59]
9	PMBA-SBA[c]	1.98×10^{-6}	EtOH/H_2O (9/1)	[60]
10	SBA-15-CA	1.5×10^{-7}	H_2O	This work

[a]8-Hydroxy-5-quinoline sulfonic acid functionalized LUS-1

[b]Bis(2-aminoethyl)-2-(9-fluorenyl)malonamide functionalized SBA-15

[c]Bis-schiff base N,N′-(1,4-phenylenedimethyli-dyne)bis(1,4-benzenediamine) (PMBA) functionalized SBA-15

Table 2 Determination of Fe^{3+} and I^- ions in different water samples using SBA-15-CA

Sample	Added amount (2 µM)	Found amount[a] (µM)	Recovery (%)
Tap water	Fe^{3+}	1.96	98
Tap water	I^-	2.01	100.5
River water	Fe^{3+}	1.92	96
Well water	I^-	1.97	98.5

[a]Results are based on three measurements

I^- ions. The emission of the resulting solutions was measured and with the help of the calibration curve, the concentration of related ions was determined. The obtained results demonstrated good agreement between the spiked and measured amount of ions.

4 Conclusion

In summary, the functionalized SBA-15 with chromotropic acid as an organic–inorganic hybrid nanomaterial (SBA-15-CA) was synthesized and characterized. The fluorescence emission properties of the probe were studied and it revealed selective detection of Fe^{3+} and I^- ions over a wide range of the related ions. SBA-15-CA was capable of detection these two opposite ions in a wide range of pH in water without using organic solvents. Furthermore, a good linearity between the fluorescence intensity of SBA-15-CA and the concentration of Fe^{3+} and I^- ions was constructed with suitable detection limits of 1.5×10^{-7} M for Fe^{3+} and 0.2×10^{-7} M for I^- ions.

Acknowledgements The authors thank the research council of University of Tehran for financial support.

Funding This research did not receive any specific grant from funding agencies in the public, commercial, or not-for-profit sectors.

References

1. A. Chmyrov, T. Sandén, J. Widengren, J. Phys. Chem. B **114**, 11282 (2010)
2. N. Kumar, V. Bhalla, M. Kumar, Coord. Chem. Rev. **257**, 2335 (2013)
3. S.K. Kim, J.L. Sessler, Chem. Soc. Rev. **39**, 3784 (2010)
4. R. Martínez-Máñez, F. Sancenón, Chem. Rev. **103**, 4419 (2003)
5. H. Zhu, J. Fan, B. Wang, X. Peng, Chem. Soc. Rev. **44**, 4337 (2015)
6. M. Wenzel, J.R. Hiscock, P.A. Gale, Chem. Soc. Rev. **41**, 480 (2012)
7. R.A. Bissell, A.P. de Silva, H.N. Gunaratne, P.M. Lynch, G.E. Maguire, C.P. McCoy, S.K. Sandanayake, *Photoinduced Electron Transfer V* (Springer, Berlin, 1993), p. 223
8. E. Beutler, V. Felitti, T. Gelbart, N. Ho, Drug Metab. Dispos. **29**, 495 (2001)
9. W.A. Jefferies, D.L. Dickstein, M. Ujiie, J. Alzheimer's Dis. **3**, 339 (2001)
10. F.L. Martin, S.J. Williamson, K.E. Paleologou, R. Hewitt, O. El-Agnaf, D. Allsop, J. Neurochem. **87**, 620 (2003)
11. G. Aumont, J.-C. Tressol, Analyst **111**, 841 (1986)
12. D. Nacapricha, P. Sangkarn, C. Karuwan, T. Mantim, W. Waiyawat, P. Wilairat, T. Cardwell, I. McKelvie, N. Ratanawimarnwong, Talanta **72**, 626 (2007)
13. F. Azizi, M. Hedayati, M. Rahmani, R. Sheikholeslam, S. Allahverdian, N. Salarkia, J. Endocrinol. Invest. **28**, 23 (2005)
14. G.-P. Tao, Q.-Y. Chen, X. Yang, K.-Y. Wang, Dyes Pigm. **95**, 338 (2012)

15. A. Goel, S. Umar, P. Nag, A. Sharma, L. Kumar, Z. Hossain, J.R. Gayen, A. Nazir, Chem. Commun. **51**, 5001 (2015)
16. M. Wang, G. Meng, Q. Huang, Q. Xu, G. Liu, Anal. Methods **4**, 2653 (2012)
17. J. Liu, Y.-Q. Xie, Q. Lin, B.-B. Shi, P. Zhang, Y.-M. Zhang, T.-B. Wei, Sens. Actuators B **186**, 657 (2013)
18. Z.B. Shang, Y. Wang, W.J. Jin, Talanta **78**, 364 (2009)
19. Z. Li, H. Yu, T. Bian, Y. Zhao, C. Zhou, L. Shang, Y. Liu, L.-Z. Wu, C.-H. Tung, T. Zhang, J. Mater. Chem. C **3**, 1922 (2015)
20. M. Zhang, B.-C. Ye, Chem. Commun. **48**, 3647 (2012)
21. C. Yi, B. Song, W. Tian, X. Cui, Q. Qi, W. Jiang, Z. Qi, Y. Sun, Tetrahedron Lett. **55**, 5119 (2014)
22. D.T. Quang, J.S. Kim, Chem. Rev. **110**, 6280 (2010)
23. K.B. Kim, H. Kim, E.J. Song, S. Kim, I. Noh, C. Kim, Dalton Trans. **42**, 16569 (2013)
24. T.-B. Wei, P. Zhang, B.-B. Shi, P. Chen, Q. Lin, J. Liu, Y.-M. Zhang, Dyes Pigm. **97**, 297 (2013)
25. G.-y. Gao, W.-j. Qu, B.-b. Shi, P. Zhang, Q. Lin, H. Yao, W.-l. Yang, Y.-m. Zhang, T.-b. Wei, Spectrochim. Acta Part A **121**, 514 (2014)
26. Z. Aydin, Y. Wei, M. Guo, Inorg. Chem. Commun. **20**, 93 (2012)
27. Y.R. Bhorge, H.-T. Tsai, K.-F. Huang, A.J. Pape, S.N. Janaki, Y.-P. Yen, Spectrochim. Acta Part A **130**, 7 (2014)
28. N. Singh, D.O. Jang, Org. Lett. **9**, 1991 (2007)
29. M. Vetrichelvan, R. Nagarajan, S. Valiyaveettil, Macromolecules **39**, 8303 (2006)
30. H.J. Jung, N. Singh, D.Y. Lee, O.D. Jang, Tetrahedron Lett. **51**, 3962 (2010)
31. T. Asefa, C.T. Duncan, K.K. Sharma, Analyst **134**, 1980 (2009)
32. E. Rampazzo, E. Brasola, S. Marcuz, F. Mancin, P. Tecilla, U. Tonellato, J. Mater. Chem. **15**, 2687 (2005)
33. S.A. El-Safty, M.A. Shenashen, Sens. Actuators B **183**, 58 (2013)
34. R. Gong, H. Mu, Y. Sun, X. Fang, P. Xue, E. Fu, J. Mater. Chem. B **1**, 2038 (2013)
35. H. Lou, Y. Zhang, Q. Xiang, J. Xu, H. Li, P. Xu, X. Li, Sens. Actuators B **166**, 246 (2012)
36. M. Karimi, A. Badiei, N. Lashgari, J. Afshani, G.M. Ziarani, J. Lumin. **168**, 1 (2015)
37. M. Ghaedi, K. Mortazavi, M. Montazerozohori, A. Shokrollahi, M. Soylak, Mater. Sci. Eng. C **33**, 2338 (2013)
38. P. Bermejo-Barrera, A. Moreda-Pineiro, M. Aboal-Somoza, J. Moreda-Pineiro, A. Bermejo-Barrera, J. Anal. At. Spectrom. **9**, 483 (1994)
39. B. Michalke, H. Witte, J. Trace Elem. Med. Biol. **29**, 63 (2015)
40. N. Krebs, C. Langkammer, W. Goessler, S. Ropele, F. Fazekas, K. Yen, E. Scheurer, J. Trace Elem. Med. Biol. **28**, 1 (2014)
41. M. Lu, R.G. Compton, Electroanalysis **25**, 1123 (2013)
42. L. Yang, L. Zou, G. Li, B. Ye, Talanta **147**, 634 (2016)
43. M. Karimi, A. Badiei, G.M. Ziarani, J. Fluoresc. **25**, 1297 (2015)
44. J. Afshani, A. Badiei, M. Karimi, N. Lashgari, G.M. Ziarani, J. Fluoresc. **26**, 263 (2016)
45. J. Afshani, A. Badiei, N. Lashgari, G.M. Ziarani, RSC Adv. **6**, 5957 (2016)
46. M. Karimi, A. Badiei, G.M. Ziarani, Inorg. Chim. Acta **450**, 346 (2016)
47. M. Karimi, A. Badiei, G.M. Ziarani, RSC Adv. **5**, 36530 (2015)
48. N. Lashgari, A. Badiei, G.M. Ziarani, J. Phys. Chem. Solids **103**, 238 (2017)
49. H.I. Lee, J.H. Kim, G.D. Stucky, Y. Shi, C. Pak, J.M. Kim, J. Mater. Chem. **20**, 8483 (2010)
50. J. Mondal, A. Modak, M. Nandi, H. Uyama, A. Bhaumik, RSC Adv. **2**, 11306 (2012)
51. P. Zarabadi-Poor, A. Badiei, A.A. Yousefi, J. Barroso-Flores, J. Phys. Chem. C **117**, 9281 (2013)
52. J.R. Lakowicz, *Principles of Fluorescence Spectroscopy* (Springer Science & Business Media, New York, 2013)
53. D.Y. Lee, N. Singh, O.D. Jang, Tetrahedron Lett. **51**, 1103 (2010)
54. W. Lin, L. Long, L. Yuan, Z. Cao, J. Feng, Anal. Chim. Acta **634**, 262 (2009)
55. K. Velmurugan, J. Prabhu, L. Tang, T. Chidambaram, M. Noel, S. Radhakrishnan, R. Nandhakumar, Anal. Methods **6**, 2883 (2014)
56. Z. Yang, M. She, B. Yin, J. Cui, Y. Zhang, W. Sun, J. Li, Z. Shi, J. Org. Chem. **77**, 1143 (2012)
57. L. Zhao, X. Xin, P. Ding, A. Song, Z. Xie, J. Shen, G. Xu, Anal. Chim. Acta **926**, 99 (2016)
58. N. Lashgari, A. Badiei, G. Mohammadi Ziarani, J. Fluoresc. **26**, 1885 (2016)
59. M. Yadavi, A. Badiei, J. Fluoresc. **24**, 523 (2014)
60. J.-Q. Wang, L. Huang, M. Xue, Y. Wang, L. Gao, J.H. Zhu, Z. Zou, J. Phys. Chem. C **112**, 5014 (2008)
61. Y. Xiang, A. Tong, Org. Lett. **8**, 1549 (2006)
62. R. Nudelman, O. Ardon, Y. Hadar, Y. Chen, J. Libman, A. Shanzer, J. Med. Chem. **41**, 1671 (1998)
63. K. Bowman-James, A. Bianchi, E. García-Espana, *Anion Coordination Chemistry* (Wiley, Weinheim, 2012)
64. B.L. Schottel, H.T. Chifotides, K.R. Dunbar, Chem. Soc. Rev. **37**, 68 (2008)